Generalized multistability and its control in a laser

Cite as: Chaos **32**, 083111 (2022); https://doi.org/10.1063/5.0093727
Submitted: 30 March 2022 • Accepted: 09 May 2022 • Published Online: 08 August 2022

Riccardo Meucci, Jean Marc Ginoux, Mahtab Mehrabbeik, et al.

Chaos ARTICLE scitation.org/journal/cha

Generalized multistability and its control in a laser

Cite as: Chaos **32**, 083111 (2022); doi: 10.1063/5.0093727
Submitted: 30 March 2022 · Accepted: 9 May 2022 ·
Published Online: 8 August 2022

Riccardo Meucci,[1,a)] Jean Marc Ginoux,[2] Mahtab Mehrabbeik,[3] Sajad Jafari,[3,4] and Julien Clinton Sprott[5]

AFFILIATIONS

[1]Istituto Nazionale di Ottica—CNR, Largo E. Fermi 6, 50125 Firenze, Italy
[2]Laboratoire CPT, Université de Toulon, CS 60584, 83041 Toulon Cedex 9, France
[3]Department of Biomedical Engineering, Amirkabir University of Technology (Tehran Polytechnic), Tehran 159163-4311, Iran
[4]Health Technology Research Institute, Amirkabir University of Technology (Tehran Polytechnic), Tehran 159163-4311, Iran
[5]Department of Physics, University of Wisconsin, 1150 University Avenue Madison, Madison, Wisconsin 53706-1390, USA

[a)]**Author to whom correspondence should be addressed:** riccardo.meucci@ino.cnr.it

ABSTRACT

We revisit the laser model with cavity loss modulation, from which evidence of chaos and generalized multistability was discovered in 1982. Multistability refers to the coexistence of two or more attractors in nonlinear dynamical systems. Despite its relative simplicity, the adopted model shows us how the multistability depends on the dissipation of the system. The model is then tested under the action of a secondary sinusoidal perturbation, which can remove bistability when a suitable relative phase is chosen. The surviving attractor is the one with less dissipation. This control strategy is particularly useful when one of the competing attractors is a chaotic attractor.

We revisit the dynamics of a simple model used to describe the first experimental evidence of chaos in a modulated laser. This pioneering experiment had an enormous impact on the scientific community, considering that a laser could also emit in a chaotic way while retaining its optical coherence properties. Lasers, particularly class B-lasers, like the CO_2 and later semiconductor lasers, have become reliable devices for studying chaos and generalized multistability. Nowadays, the latter phenomenon is widely investigated in the most diverse fields, sharing the possibility of jumping between the different attractors using small perturbations. The model is characterized in terms of its dissipativity. A novel aspect of the present investigation is the stability analysis in an increased dimension phase space allowing analytic treatment.

I. INTRODUCTION

Exactly 40 years have passed since the pioneering experiment on deterministic chaos and generalized multistability in a CO_2 laser with periodic modulation of the cavity losses.[1] These two issues have profoundly influenced and motivated research in different fields of laser physics. Let us consider multistability, that is, the coexistence of different stable states in nonlinear systems (for two review papers on the subject, see Refs. 2 and 3). This means that a dissipative dynamical system can have more solutions for equal values of the control parameters depending only on the values of initial conditions. The set of initial conditions (more precisely, the closure of it) leading, in the long term limit, to a given attractor is called the basin of attraction, whose structure can be fractal. The complicated structure of basin boundaries in multistable systems determines their sensitivity to noise and periodic perturbations. This makes them attractive for controlling techniques allowing the switching from one attractor to another one. Many dynamical systems exhibit multistability, including laser physics,[4,5] neuroscience,[6] chemical reactions,[7] climate systems,[8] and biological and ecological ones.[9]

In the 1982 seminal paper,[1] a simple two-level laser model was used. A few years later, a five-dimensional model was introduced, accounting for the interaction between the electromagnetic field and a molecular model where the two lasing levels are coupled to two rotational manifolds. Using the center manifold theory, it is possible to reduce the five-dimensional model to a two-dimensional model by adding suitable nonlinear corrections, as demonstrated by

Ciofini *et al.*[10] However, considering that the key nonlinearity is the same in the two models, it often is preferable to use the two-level model. Very recently, a simple three-dimensional laser model was proposed to investigate the instabilities of the laser with feedback. Such a model possesses the minimal and essential nonlinearities as the Rossler, Lorenz, Chua, and Chen models.[11,12] The two-level model that we use here simply derives from it by eliminating the feedback equation and introducing a sinusoidal modulation of the cavity losses parameter and recapturing the basic scheme of the one introduced in Ref. 1. In such a case, a certain flexibility is used in the γ parameter, which accounts for the relaxation rate of population inversion.

Increasing interest has been posed in generalized multistability and its control, considering the possibility of using small perturbations to select one of the competing solutions (see the review paper by Pisarchik and Feudel[13]). Control of multistability applying small perturbation without phase shift was first introduced in the dissipative Hénon map,[14,15] later applied to a semiconductor laser,[16] and experimentally demonstrated in a fiber laser[17] and in coupled oscillators.[18] The role of the phase of additional harmonic perturbation was first considered by Egorov and Koronovskii[19] in the dissipative Hénon map. So, to the best of our knowledge, applying this control method to a laser model has not been performed yet. Here, we consider the key role of the phase difference between the main driving frequency responsible for the chaos and multistability (f_{mod}) and a secondary sinusoidal perturbation for its control (f_{pert}). The attention is here focused on the resonant case where $f_{mod} = f_{pert}$.[20,21] The paper is organized as follows: In Se. II, we introduce the two-level laser model and its time-rescaled version. Numerical results showing evidence of generalized bistability are here presented. In Sec. III, we transform this two-level non-autonomous model into an autonomous four-dimensional dynamical system that enables us to provide a mathematical analysis and confirm the numerical results obtained. In Sec. IV, control of bistability is obtained by introducing a secondary sinusoidal perturbation adjusting the relative phase. Finally, a discussion of these results as well as the perspectives to be given to this work is presented in Sec. V.

II. TWO-LEVEL NON-AUTONOMOUS LASER MODEL

Starting from the seminal works of Arecchi *et al.*,[1,22,23] we propose analyzing the following *two-level laser model*:

$$\begin{aligned} \dot{x} &= -k_0 x\left[1 + k_1\left(B_0 + m\sin(2\pi f_{mod} t)\right)^2 - y\right], \\ \dot{y} &= -\gamma y - \frac{2k_0}{\alpha} xy + \gamma p_0. \end{aligned} \tag{1}$$

Here, the fast variable x is the laser intensity with a time-dependent decay rate $k(t)$ given by $k_0\left[1 + k_1\left(B_0 + m\sin(2\pi f_{mod} t)\right)^2\right]$, where k_0 is the nonmodulated cavity loss parameter and k_1 accounts for its modulation depth. $B_0 + m\sin(2\pi f_{mod} t)$ is the applied modulation signal with a bias value B_0 summed to a sinusoidal signal with amplitude m and modulation frequency f_{mod}. The slow variable y is the population inversion with a decay rate γ, while the parameter y_0 is the population inversion, imposed by the pumping process. The adopted normalization is such that the original equations[1] can be re-obtained considering $\alpha = 2k_0/\gamma$ and a threshold inversion $y_{thresh} = k_0/G$, where G is the field-matter coupling constant.[1]

A. Rescaled form

We propose the following change of variables and parameters to recast Eq. (1) in a rescaled form. Let us pose: $t \to \frac{t}{k_0}$ and

$$k = k_1, \quad f'_{mod} = \frac{f_{mod}}{k_0}, \ \gamma' = \frac{\gamma}{k_0}, \ \alpha' = \frac{2}{\alpha}.$$

By dropping $'$ for these parameters, the two-level model (1) now reads

$$\begin{aligned} \frac{dx}{dt} &= -x\left[1 + k\left(B_0 + m\sin(2\pi f_{mod} t)\right)^2 - y\right], \\ \frac{dy}{dt} &= -\gamma y - \alpha xy + \gamma p_0, \end{aligned} \tag{2}$$

where $k = 12$, $B_0 = 0.1215$, $m = 0.02$, $f_{mod} = 0.005$, $\gamma = 0.0025$, $\alpha = 0.002$, and $p_0 = 1.252$. In the following, we use B_0 as the bifurcation parameter. Numerical investigations on the nonautonomous dynamical system (2) highlight the generalized bistability and its control. After presenting these numerical results, the two-level laser model [although an attempt to relate bistability and dissipation has already been made in this system,[26] here we want to retrace it starting from the first principles; dissipativity is related to the Jacobian matrix of the model[27,28], Eq. (2)] is transformed into an autonomous four-dimensional dynamical system that allows its mathematical analysis.

B. Jacobian matrix

The phenomenon of generalized multistability, the coexistence of attractors for the same parameter values, is related to the phenomenon of crises.[24] The presence of different crises in dynamical systems depends on the amount of dissipation.[25] Although an attempt to relate bistability and dissipation has already been made in this system,[26] here we want to retrace it starting from the first principles. Dissipativity is related to the Jacobian matrix of the model.[27,28]

The Jacobian matrix of the rescaled two-level model (2) reads

$$J = \begin{pmatrix} y - k\left(B_0 + m\sin(2\pi f_{mod} t)\right)^2 - 1 & x \\ -\alpha y & -\gamma - \alpha x \end{pmatrix}. \tag{3}$$

So, the trace of the Jacobian, which represents the dissipation rate of the rescaled two-level model (2), reads

$$Tr(J) = y - k\left(B_0 + m\sin(2\pi f_{mod} t)\right)^2 - 1 - \gamma - \alpha x. \tag{4}$$

In Fig. 1(a), the bifurcation diagram of system (2), i.e., the maxima of the solution $x(t)$ as a function of B_0 (all other parameters are those given above), is plotted using the forward (yellow) and backward (blue) methods. The monostable regions, wherein the system exhibits only one dynamic, are illustrated in green color. Note that the forward–backward method is a straightforward way of detecting multistability in a system's dynamics since it helps us to remain in the basin of attraction of an attractor, or in other words, track an attractor as the bifurcation parameter varies. Therefore, different attractors can be detected by changing the bifurcation parameter in

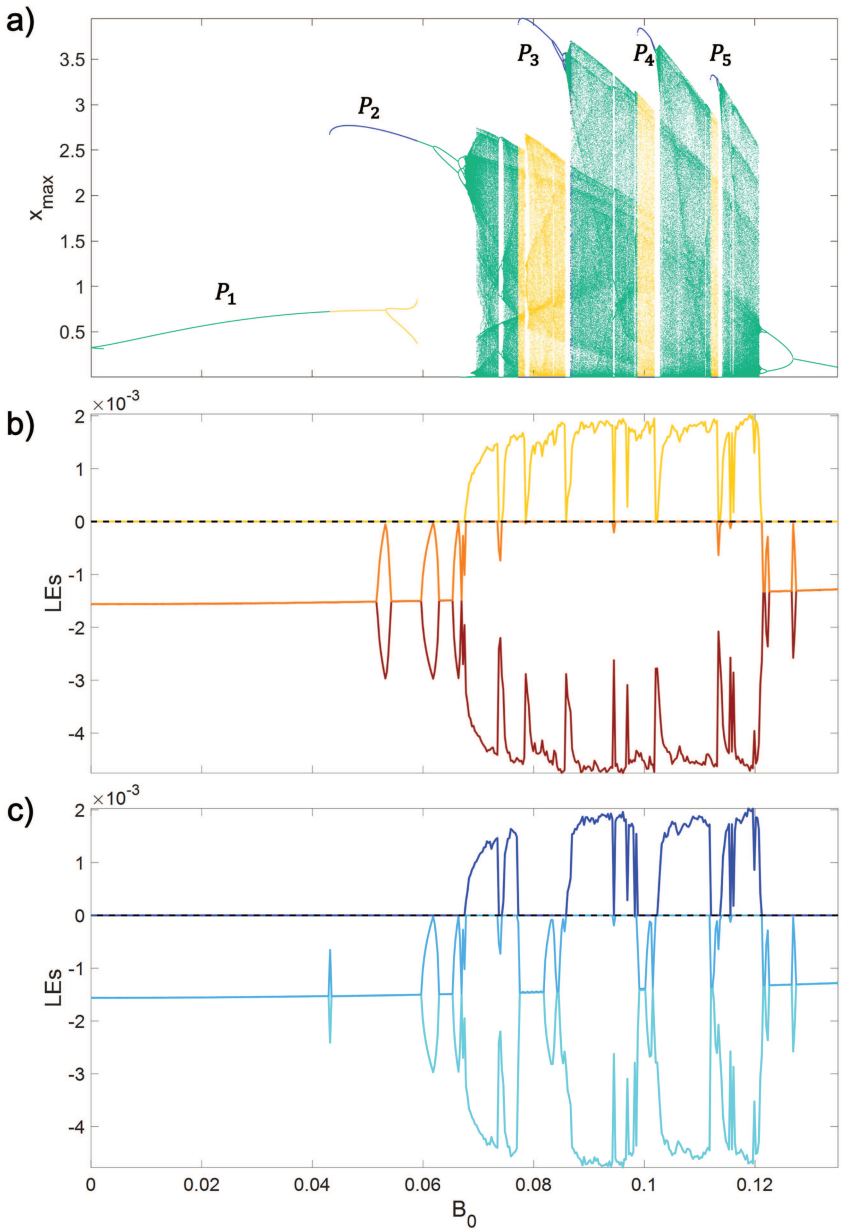

FIG. 1. (a) Forward (yellow) and backward (blue) bifurcation diagrams ($x_{max}(t)$) and the corresponding (b) forward and (c) backward LEs spectra of system (2) as a function of B_0 for $k = 12$, $m = 0.02$, $f_{mod} = 0.005$, $\gamma = 0.0025$, $\alpha = 0.002$, $p_0 = 1.252$, and $(x(0), y(0)) = (0.3, 1.0028)$. Green color indicates the regions wherein the system is monostable.

opposite directions (increasing as forward and decreasing as backward) and selecting the last variables' values of each step as the next step's initial condition.[29,30] Employing the Wolf algorithm[31] with the run-time of 1 000 000 ms, the corresponding Lyapunov exponents (LEs) for the same range of parameter B_0 are reported in Figs. 1(b) and 1(c). The LEs spectra with yellow and blue color themes, respectively, correspond to the forward (yellow) and backward (blue) bifurcation diagram [Fig. 1(a)].

As we deduce from the bifurcation diagram [Fig. 1(a)], the attractors' structure is rather complicated due to the presence of local and global bifurcations.[27,28] However, a qualitative description can be provided in terms of the five leading periodic orbits, which is present in this dynamical system (2). Such periodic solutions are labeled as $P_1, P_2, \ldots, P_5$, and each of them is characterized by the presence of a single peak every 1–5 periods of the driving frequency (f_{mod}). As the control parameter B_0 is increased, we observe that the P_2 solution is replaced by the P_1 solution due to a crisis. This solution (upper branch solution) coexists with the lower branch solution and its first subharmonic $P_{1,2}$ in the range $B_0 \in [0.0445, 0.0558]$ (first bistable window B_I). The upper branch solution P_2 loses its stability via a subharmonic bifurcation until a new crisis is encountered and replaced by a P_3 solution,

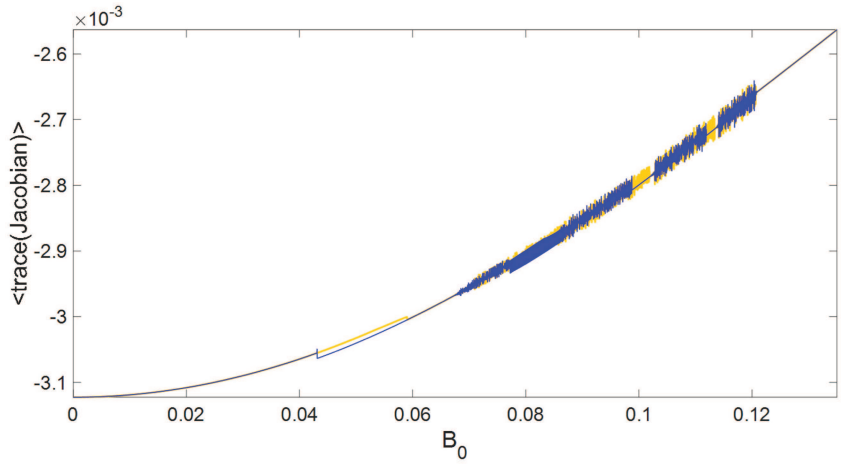

FIG. 2. Forward (yellow) and backward dissipation diagrams [$Tr(J)$ over 1 000 000 ms] of system (2) as a function of B_0 considering $k = 12$, $m = 0.02$, $f_{mod} = 0.005$, $\gamma = 0.0025$, $\alpha = 0.002$, $p_0 = 1.252$, and $(x(0), y(0)) = (0.3, 1.0028)$.

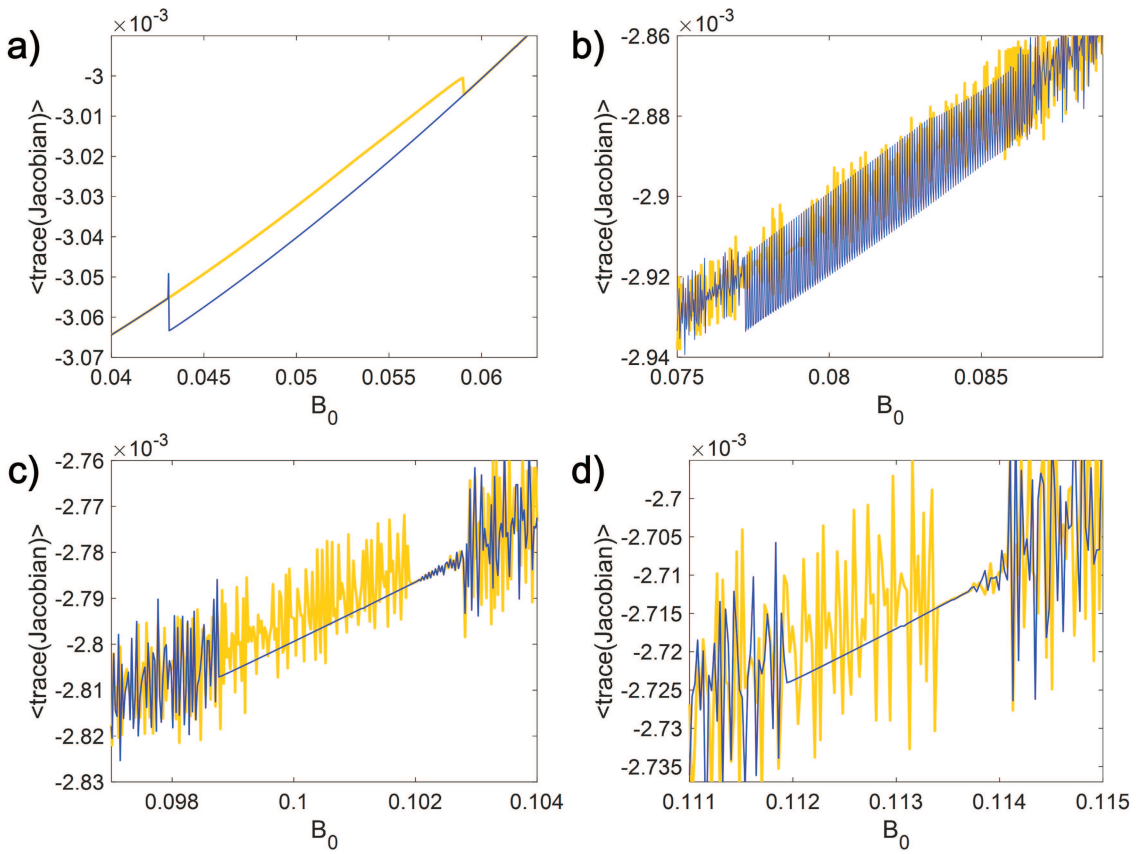

FIG. 3. Zoomed-in version of bistable regions in Fig. 2 for (a) $0.0445 < B_0 < 0.0558$, (b) $0.0776 < B_0 < 0.0858$, (c) $0.0988 < B_0 < 0.1018$, and (d) $0.1120 < B_0 < 0.1134$. The considered parameters are $k = 12$, $m = 0.02$, $f_{mod} = 0.005$, $\gamma = 0.0025$, $\alpha = 0.002$, and $p_0 = 1.252$, with the initial condition of $(x(0), y(0)) = (0.3, 1.0028)$.

which coexists with a lower branch chaotic attractor in the range $B_0 \in [0.0776, 0.0858]$ (second bistable region). This process is continued up to the appearance of the P_4 solution and the fourth bistable region around $B_0 \in [0.0988, 0.1018]$. The fourth bistability occurs at around $B_0 \in [0.1120, 0.1134]$. At $B_0 \approx 0.12$, we observe the last crisis with lower-amplitude attractors, belonging to an inverse cascade of the primary P_1 lower branch solution. The four bistable regions are identified by using forward and backward methods by scanning the bifurcation parameter in the forward and backward directions.[30] These bistable regions can also be detected in the LEs spectra [Figs. 1(b) and 1(c)] in forward and backward directions. Relevant information about the organization of the solutions is provided by the evaluation of the dissipation rate (trace of the Jacobian matrix). The corresponding dissipation diagram of the bifurcation diagram described above is shown in Fig. 2.

From Fig. 2, we can graphically deduce the bistable regions as well as in Fig. 1 (see the zoomed regions of bistability in Fig. 3). We observe that in the second bistable region B_{II}, the upper branch periodic solution P_3 is characterized by alternating between two values whose average is below the competing chaotic attractor. Figures 2 and 3 enable us to distinguish between the two coexisting solutions according to their dissipative rate. It is important to note that the upper branch solutions (periodic solutions) are characterized by lower dissipativity. Note that the yellow and blue diagrams in Figs. 2 and 3, respectively, correspond to the forward and backward bifurcation diagrams in Fig. 1(a).

In Fig. 4, the bifurcation diagram of system (2)), i.e., the maxima of the solution $x(t)$ as a function of γ (all other parameters are those given above), is plotted. From Fig. 4, we observe three bistability windows around $\gamma = 2.5 \times 10^{-3}$, $\gamma = 3.5 \times 10^{-3}$, and $\gamma = 5.5 \times 10^{-3}$. In the latter bistability window, the two coexisting solutions are period ones. From the bifurcation diagram (Fig. 4), it is also possible to identify the bifurcation regions. Similar to Fig. 1(a), the forward and backward bifurcations are demonstrated in yellow and blue colors, respectively. For better visualization, the monostable regions are plotted in green colors.

Thus, in Sec. II, we numerically show that generalized bistability [simultaneous presence of two kinds of attractors having the same values of the control parameters but different initial conditions, in our case, we only consider $x(0)$ is different] depends on either B_0 or γ for the two-level laser model (2). Such bistable regions are highlighted with the help of a new kind of *bifurcation diagrams*, presented in Sec. III. To this aim, in Sec. III, we transform this two-level non-autonomous model (2) into a four-dimensional autonomous dynamical system.

III. TWO-LEVEL AUTONOMOUS LASER MODEL

Let us notice that the presence of the $\sin(2\pi f_{mod} t)$ in the right-hand side of the first equation of the two-level model (2) makes it non-autonomous. However, recalling that a *sine* function is nothing else but the solution of a harmonic oscillator. So, let us pose

$$z(t) = B_0 + m \sin(2\pi f_{mod} t),$$

which is the solution of the following second-order ordinary differential equation (ODE):

$$\ddot{z}(t) + \omega^2 z(t) = \omega^2 B_0,$$

where $\omega = 2\pi f_{mod}$. Using the classical D'Alembert transformation,[32] this second-order ODE may be written as the following system of first-order ODEs:

$$\dot{z} = -\omega^2 u(t), \quad z(0) = B_0,$$
$$\dot{u} = z(t) - B_0, \quad u(0) = -\frac{m}{\omega}.$$

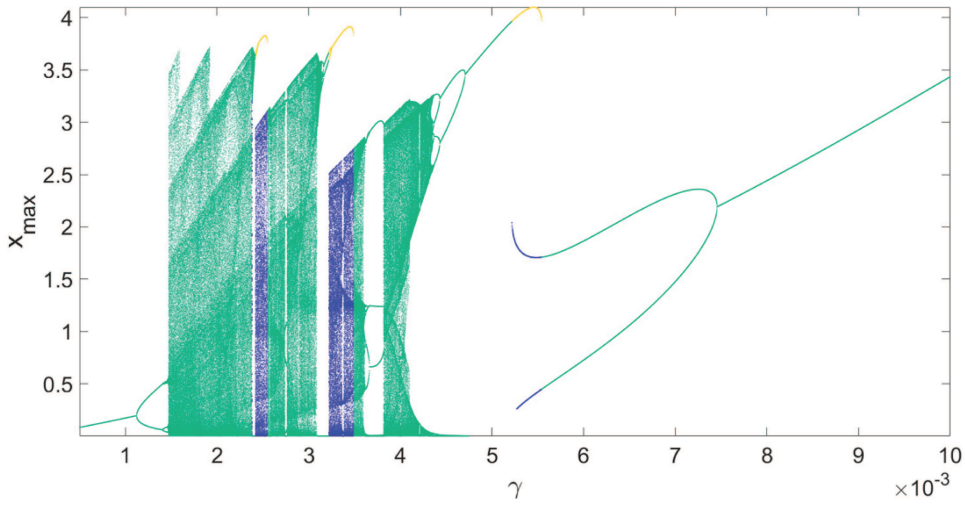

FIG. 4. Forward (yellow) and backward (blue) bifurcation diagrams ($x_{max}(t)$) of system (2) as a function of γ considering $k = 12$, $B_0 = 0.1215$, $m = 0.02$, $f_{mod} = 0.005$, $\alpha = 0.002$, $p_0 = 1.252$, and $(x(0), y(0)) = (0.3, 1.0028)$. Green color indicates the regions wherein the system is monostable.

Thus, we transform the two-level non-autonomous model (2) into an autonomous one, while increasing the dimension of two. We have

$$\begin{aligned}\dot{x} &= -x\left(1+kz^2-y\right),\\ \dot{y} &= -\gamma y-\alpha xy+\gamma p_0,\\ \dot{z} &= -\omega^2 u,\\ \dot{u} &= z-B_0,\end{aligned} \tag{5}$$

where $k=12$, $B_0=0.1215$, $m=0.02$, $f_{mod}=0.005$, $\omega=2\pi f_{mod}$, $\gamma=0.0025$, $\alpha=0.002$, and $p_0=1.252$. The initial conditions $z(0)=B_0$ and $u(0)=-m/\omega$ are imposed to $z(t)$ and $u(t)$.

A. Fixed points

Using the classical nullcline method, it can be shown that the dynamical system (5) admits two fixed points,

$$I_1\left(0,p_0,B_0,0\right); I_2\left(-\frac{\gamma}{\alpha}\frac{1+kB_0^2-p_0}{1+kB_0^2}, 1+kB_0^2, 0, 0\right). \tag{6}$$

B. Jacobian matrix

The Jacobian matrix of the dynamical system (5) reads

$$J=\begin{pmatrix}-(1+kz^2-y) & x & -2kxz & 0\\ -\alpha y & -\gamma-\alpha x & 0 & 0\\ 0 & 0 & 0 & -\omega^2\\ 0 & 0 & 1 & 0\end{pmatrix}. \tag{7}$$

Replacing the coordinate of the fixed points I_1 (6) in the Jacobian matrix (7), four following eigenvalues are obtained:

$$\lambda_1=-\gamma, \quad \lambda_2=-\left(1+kB_0^2-p_0\right), \ \lambda_{3,4}=\pm i\omega. \tag{8}$$

Considering $-(1+kB_0^2-p_0)>0$, λ_2 is real and positive while λ_1 is real and negative. Hence, according to the Lyapunov theorem, the fixed point I_1 is *unstable*.

Replacing the coordinate of the fixed points I_2 (6) in the Jacobian matrix (7), four following eigenvalues are obtained:

$$\lambda_{1,2}=-\frac{\gamma p_0}{2y^*}\pm\frac{\sqrt{\Delta}}{2} \quad \text{and} \quad \lambda_{3,4}=\pm i\omega, \tag{9}$$

where

$$\Delta=\left(\frac{\gamma p_0}{y^*}\right)^2+4\gamma(y^*-p_0) \quad \text{with} \quad y^*=1+kB_0^2.$$

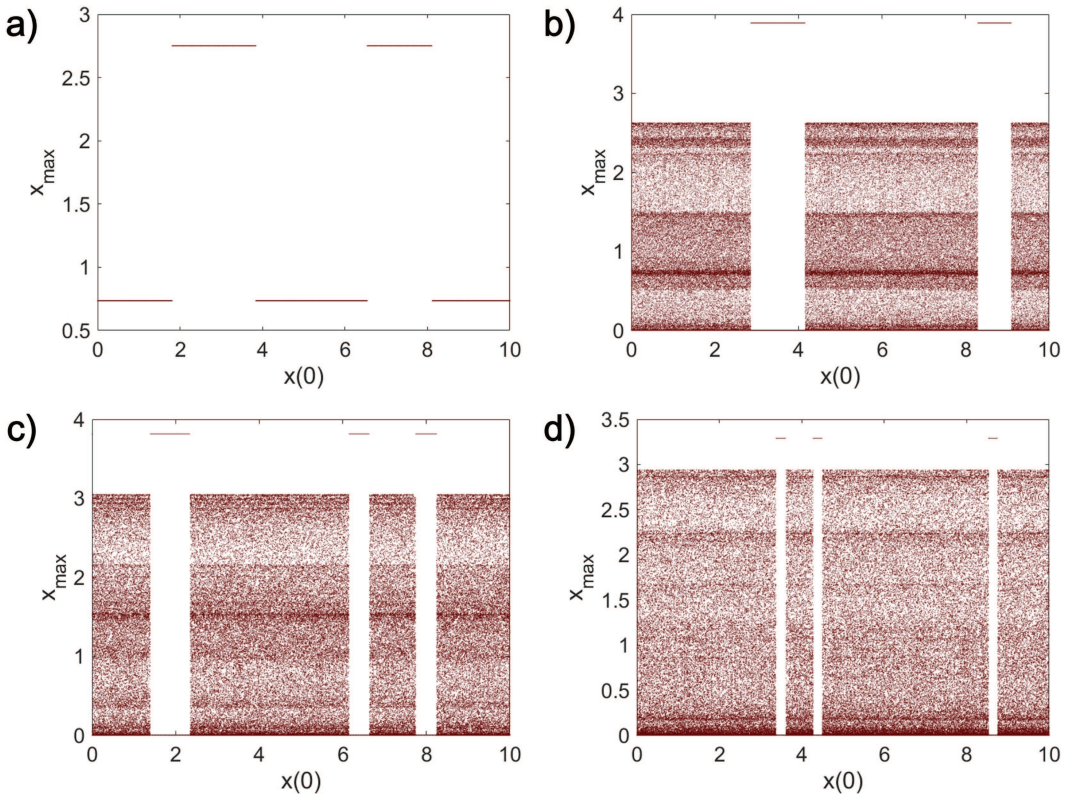

FIG. 5. Bifurcation diagram ($x_{max}(t)$) of system (5) as a function of the initial condition $x(0)$ assuming $y(0)=1$, $k=12$, $m=0.02$, $f_{mod}=0.005$, $\omega=2\pi f_{mod}$, $\gamma=0.0025$, $\alpha=0.002$, and $p_0=1.252$ for (a) $B_0=0.05$, (b) $B_0=0.08$, (c) $B_0=0.1$, and (d) $B_0=0.112$.

Assuming the same set of parameters, $\Delta < 0$ and both real parts $\gamma p_0/y^*$ in $\lambda_{1,2}$ are negative. Hence, according to the Lyapunov theorem, the fixed point I_2 is *stable*. Notice that a Hopf bifurcation can only occur if and only if $p_0 = 0$. Nevertheless, in such a case, Δ would become positive. Therefore, no Hopf bifurcations can occur in system (5). It is important to note that the emergence of chaos is related to the interplay between the two stationary points. The unstable fixed point I_1 provides the re-injection to I_2, allowing time evolution of the trajectory in the phase space.

Now, let us highlight the bistable regions of system (5) and so of the two-level model (2). To this aim, we propose to use *bistability bifurcation diagrams* by plotting (as usual) the maxima of the variable $x(t)$ as a function of the initial condition $x(0)$ instead of the control parameter B_0, which is fixed here. Figure 5 represents such bifurcation diagrams for $B_0 = 0.05$, $B_0 = 0.08$, $B_0 = 0.1$, and $B_0 = 0.112$.

Figure 5 highlights the existence of two different regions of stability for the attractor solution of system (5). In the following, we consider that the lower branch corresponds to the first stability region while the upper branch corresponds to the second. As an example, from Fig. 5(a) ($B_0 = 0.05$), we deduce that for $x(0) = 1$, the attractor is in the lower branch [yellow attractor corresponds to the yellow bifurcation in Fig. 1(a)], and the solution is a periodic solution with one peak for the $x(t)$. For $x(0) = 3$, the attractor is in the upper branch [blue attractor corresponds to the blue bifurcation in Fig. 1(a)], and the solution is a P_2 solution [see Fig. 6(a)]. From Fig. 5(b) ($B_0 = 0.08$), we find that for $x(0) = 1$, the attractor is in the lower branch (shown in yellow) and the solution is chaotic. For $x(0) = 3$, the attractor is in the upper branch (shown in blue), and the periodic solution is a P_3 solution [see Fig. 6(b)]. From Fig. 5(c) ($B_0 = 0.1$), we find that for $x(0) = 1$, the attractor is in the lower branch (shown in yellow) and the solution is chaotic. For $x(0) = 2$, the attractor is in the upper branch (shown in blue), and the periodic solution is a P_4 [see Fig. 6(c)]. From Fig. 5(d) ($B_0 = 0.112$), we find that for $x(0) = 3.5$, the attractor is in the upper branch (shown in blue) and the periodic solution is a P_5. For $x(0) = 4$, the attractor is in the lower branch (shown in yellow), and the solution is chaotic [see Fig. 6(d)]. Notice that both attractors coexist in all these cases. The basins of attraction corresponding to the four bistable regions are reported in Fig. 7, wherein the yellow and blue colors denote the yellow and blue diagrams in Fig. 1(a) and the attractors of the same color in Fig. 6. Although the basins of attraction provide general information about the organization of the phase space, we consider the representation in terms of bistability bifurcation diagrams easier to be interpreted.

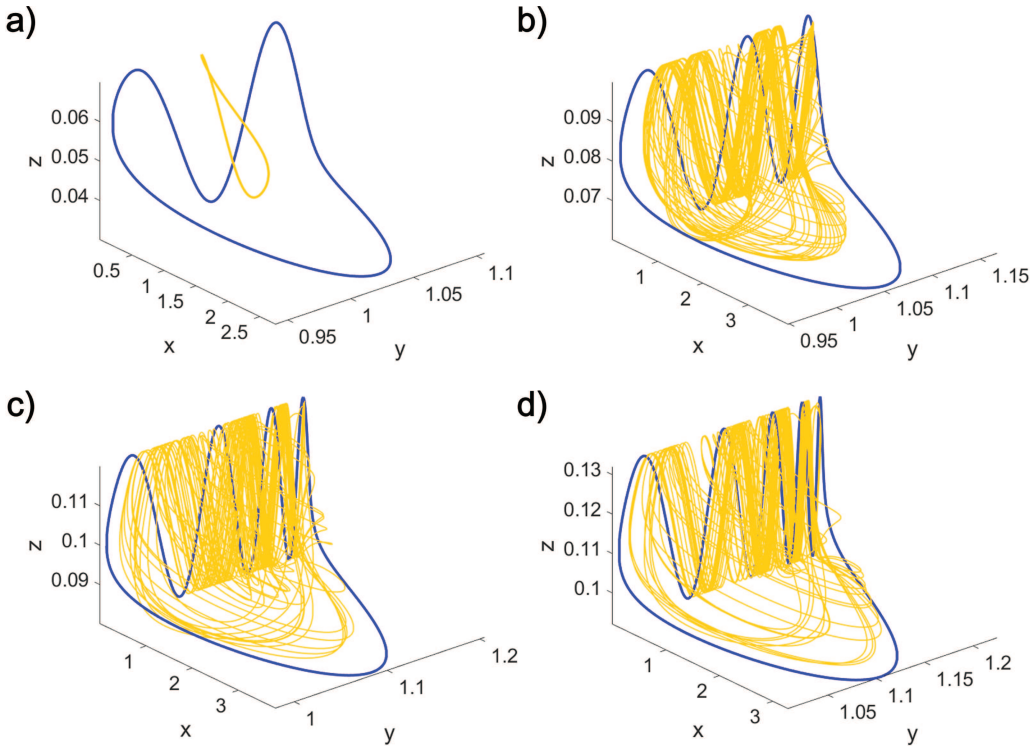

FIG. 6. Phase portraits of system (5) in the *xyz*-space for (a) $B_0 = 0.05$, $(x(0), y(0)) = (1, 1)$ (yellow), and $(x(0), y(0)) = (3, 1)$ (blue), (b) $B_0 = 0.08$, $(x(0), y(0)) = (1, 1)$ (yellow), and $(x(0), y(0)) = (3, 1)$ (blue), (c) $B_0 = 0.1$, $(x(0), y(0)) = (1, 1)$ (yellow), and $(x(0), y(0)) = (2, 1)$ (blue), and (d) $B_0 = 0.112$, $(x(0), y(0)) = (4, 1)$ (yellow), and $(x(0), y(0)) = (3.5, 1)$ (blue). Other parameters are $(z(0), u(0)) = (B_0, -m/\omega)$, $k = 12$, $m = 0.02$, $f_{mod} = 0.005$, $\omega = 2\pi f_{mod}$, $\gamma = 0.0025$, $\alpha = 0.002$, and $p_0 = 1.252$. Note that the yellow and blue attractors correspond to the bistable regions (with the same colors) in Fig. 1(a).

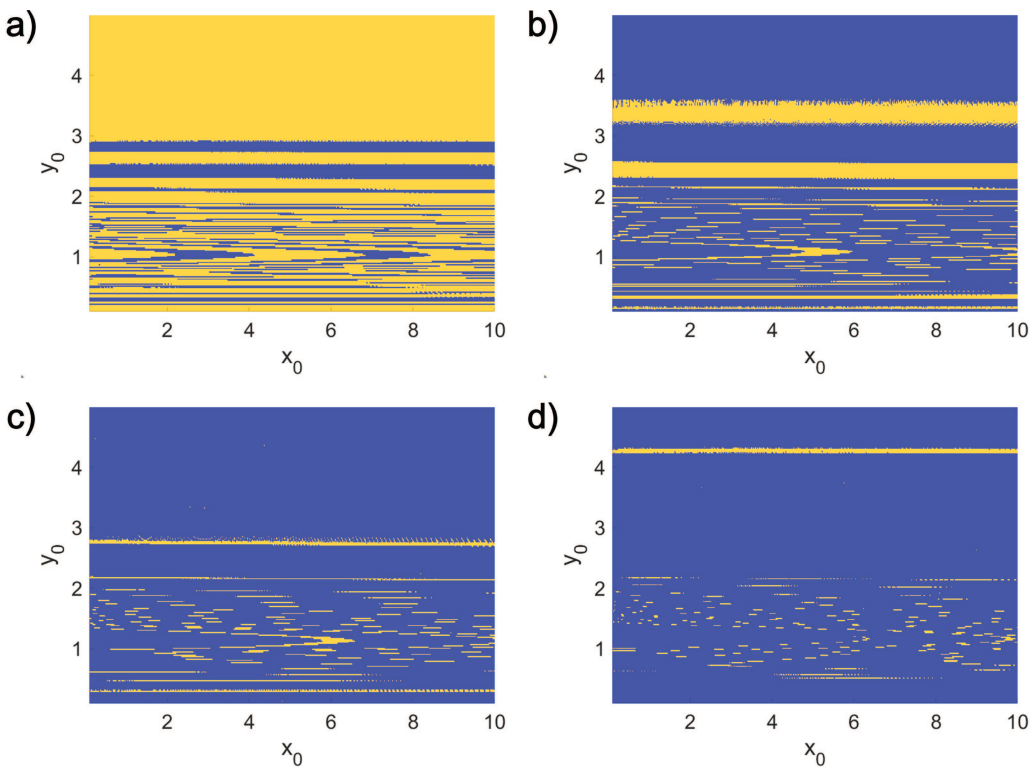

FIG. 7. Basins of attraction of system (5) for (a) $B_0 = 0.05$, (b) $B_0 = 0.08$, $B_0 = 0.1$, and (d) $B_0 = 0.112$. The predetermined parameters are $k = 12$, $m = 0.02$, $f_{mod} = 0.005$, $\omega = 2\pi f_{mod}$, $\gamma = 0.0025$, $\alpha = 0.002$, and $p_0 = 1.252$. Yellow and blue colors correspond to the attractors of the same color in Fig. 6.

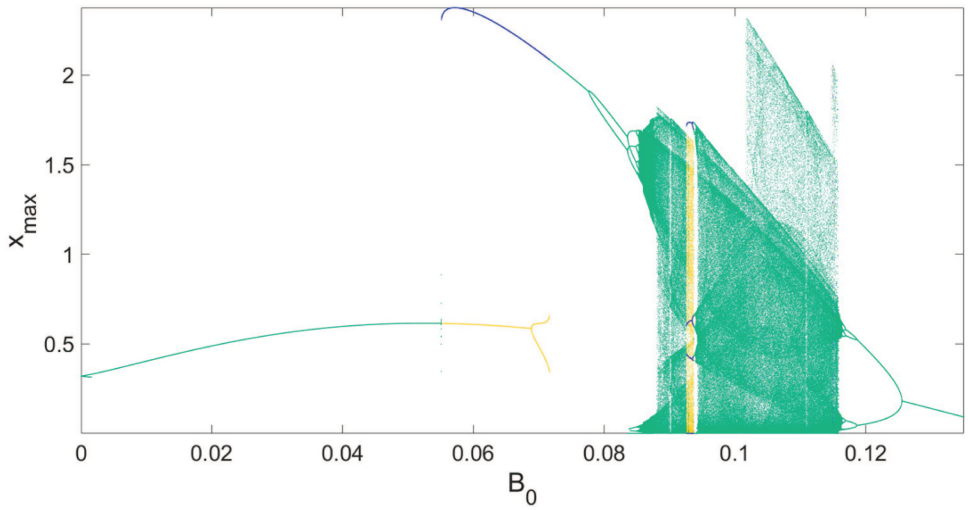

FIG. 8. Forward (yellow) and backward (blue) bifurcation diagrams ($x_{max}(t)$) of system (10) as a function of B_0 considering $k = 12$, $m = 0.02$, $\varepsilon = 0.0006$, $\varphi = \pi$, $f_{mod} = 0.005$, $\gamma = 0.0025$, $\alpha = 0.002$ $p_0 = 1.252$, and $(x(0), y(0)) = (0.3, 1.0028)$. Green color indicates the regions wherein the system is monostable.

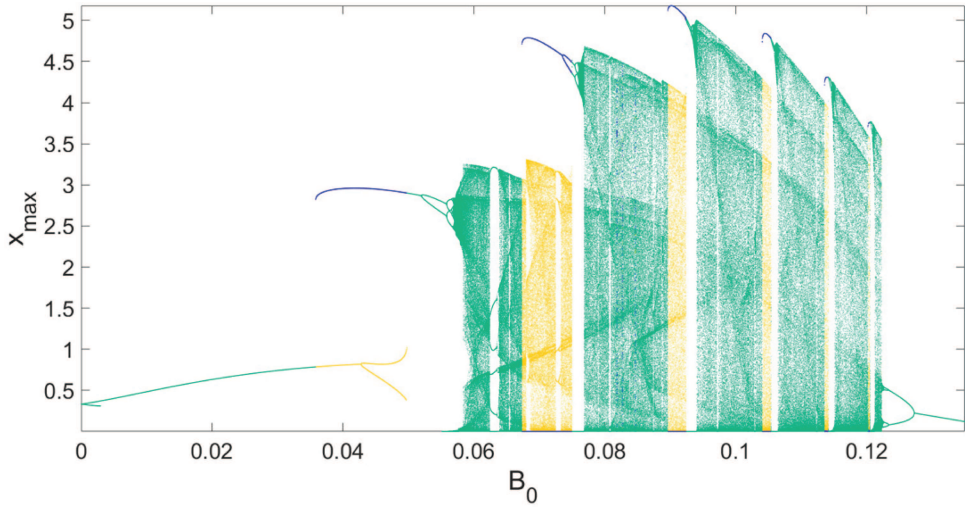

FIG. 9. Forward (yellow) and backward (blue) bifurcation diagrams ($x_{max}(t)$) of system (10) as a function of B_0 considering $k = 12$, $m = 0.02$, $\varepsilon = 0.0006$, $\varphi = 0$, $f_{mod} = 0.005$, $\gamma = 0.0025$, $\alpha = 0.002$, $p_0 = 1.252$, and $(x(0), y(0)) = (0.3, 1.0028)$. Green color indicates the regions wherein the system is monostable.

IV. CONTROL OF GENERALIZED MULTISTABILITY

Let us consider the effects of a second sinusoidal perturbation with the amplitude ε smaller than m in the two-level non-autonomous model (2). Consequently, the dynamics is now described by

$$\dot{x} = -x\left[1 + k\left(B_0 + \varepsilon \sin(2\pi f_{mod} t + \varphi) + m \sin(2\pi f_{mod} t)\right)^2 - y\right], \tag{10}$$

$$\dot{y} = -\gamma y - \alpha x y + \gamma p_0,$$

where $k = 12$, $B_0 = 0.0832$, $m = 0.02$, $\varepsilon = 0.0006$, $f_{mod} = 0.005$, $\gamma = 0.0025$, $\alpha = 0.002$, and $p_0 = 1.252$. Bistability can be removed by accurately choosing ε and phase difference φ, as illustrated in Fig. 8. In such a case, the optimal value for the phase difference φ is around $\pi = 3.1415$. The opposite effect occurs when $\varphi = 0 = 2\pi$, as shown in Fig. 9. Removing bistability means stabilizing the lower-amplitude attractors, which are less dissipative than the upper branch solutions (see the yellow and blue traces in Fig. 8).

From a comparison with the unperturbed bifurcation diagram shown in Fig. 1, we see that the controlling perturbation critically affects the dynamics by delaying the occurrence of the first bifurcation window to a value of the control parameter B_0, where the unperturbed dynamics is chaotic. Furthermore, we note that, for $\varepsilon = 0.006$, which implies a relative perturbation strength $\varepsilon/m = 0.006/0.02 = 30\%$, the unperturbed bistability window, centered around $B_0 = 0.05$, is shifted around $B_0 = 0.06$. Here, several considerations can be drawn. First, if the competing solutions are periodic, as in the first bistability window, we need to use a greater perturbation with respect to the case where the lower branch

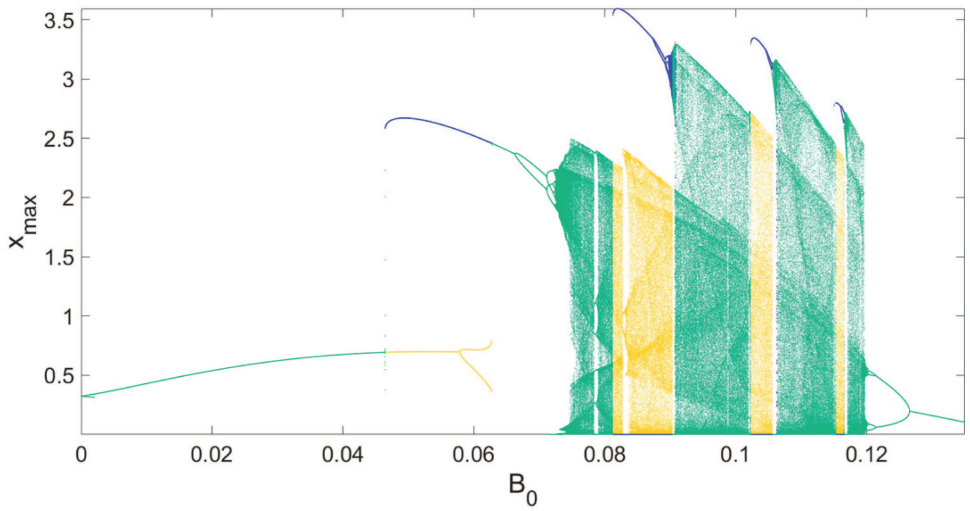

FIG. 10. Forward (yellow) and backward (blue) bifurcation diagrams ($x_{max}(t)$) of system (10) as a function of B_0 considering $k = 12$, $m = 0.02$, $\varepsilon = 0.0002$, $\varphi = \pi$, $f_{mod} = 0.005$, $\gamma = 0.0025$, $\alpha = 0.002$ $p_0 = 1.252$, and $(x(0), y(0)) = (0.3, 1.0028)$. Green color indicates the regions wherein the system is monostable.

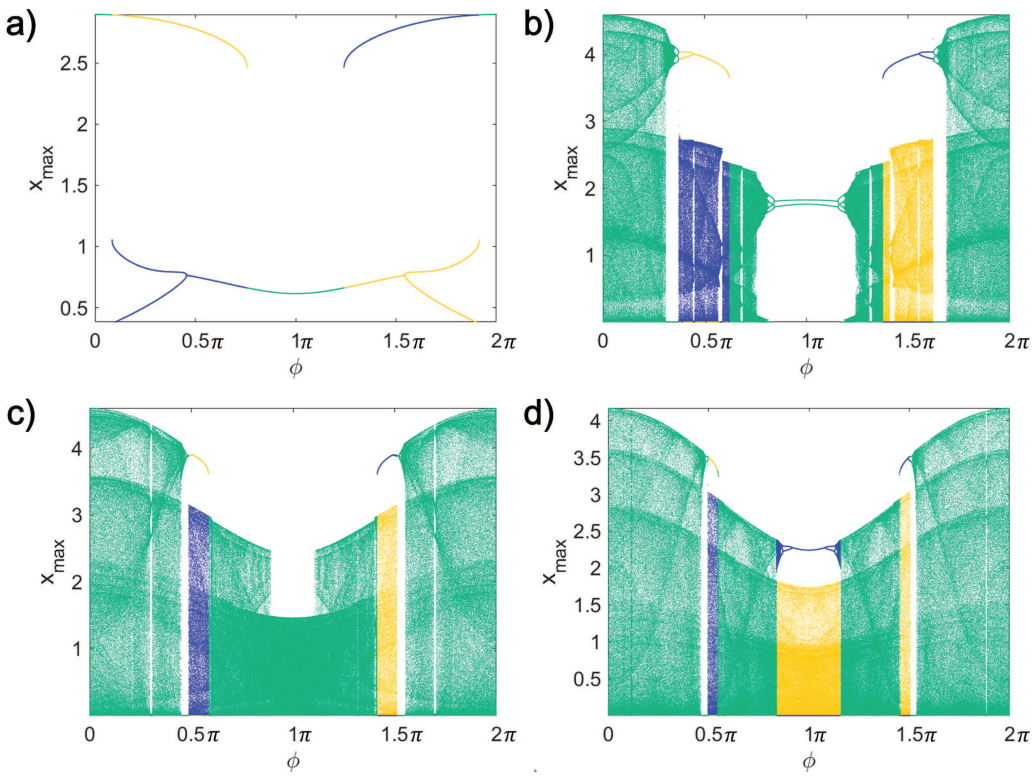

FIG. 11. Forward (yellow) and backward (blue) bifurcation diagrams ($x_{max}(t)$) of system (10) as a function of φ for (a) $B_0 = 0.05$, (b) $B_0 = 0.08$, (c) $B_0 = 0.1$, and (d) $B_0 = 0.112$, considering $k = 12$, $m = 0.02$, $\varepsilon = 0.0006$, $f_{mod} = 0.005$, $\gamma = 0.0025$, $\alpha = 0.002$ $p_0 = 1.252$, and $(x(0), y(0)) = (0.3, 1.0028)$. Green color indicates the regions wherein the system is monostable.

solution is chaotic, and the upper branch is periodic. From Fig. 8, we clearly see that the first bistability window is shifted in the forward B_0 direction, but the other bistability windows are removed except the small one around $B_0 = 0.09$. This is consistent with the fact that the width of the bistable regions diminishes as B_0 is increased.

In Fig. 9, where the wrong phase difference φ is chosen, we clearly see that the first bistability window and the other ones are anticipated with respect to the bifurcation parameter B_0. We also observe that their width is increased when compared with the unperturbed case of Fig. 1.

As the perturbation strength ε is reduced (keeping the right phase difference φ), we observe that the adopted strategy for controlling bistability remains valid but in restricted regions of the unperturbed bistable regions. This fact emerges from Fig. 10, where the relative perturbation strength is $\varepsilon/m = 0.002/0.02 = 10\%$.

Keeping the same parameters values, Fig. 11 provides the forward (yellow) and backward (blue) bifurcation diagrams with respect to the variation of phase φ and four values of B_0 in the four bistable regions, i.e., $B_0 = 0.05$, $B_0 = 0.08$, $B_0 = 0.1$, and $B_0 = 0.112$. According to Fig. 11, $\varphi = \pi$ is a proper phase difference to control the bistability for $B_0 = 0.05$, $B_0 = 0.08$, and $B_0 = 0.1$. However, it is a wrong phase difference to control bistability for $B_0 = 0.112$. Hence, Fig. 11 can help to find a proper phase difference for a set of parameters' values.

It should be noted that, in Figs. 8–10, the yellow and blue colors refer to the forward and backward diagrams in bistable regions, and the green color shows the monostable regions.

V. CONCLUSION

The original two-dimensional laser model that gave evidence of chaos and generalized multistability was revisited. The considered model shows how the relaxation rates of the two variables, laser intensity and population inversion, were crucial for the observation of multistability. In particular, by adjusting the cavity loss parameter (the only accessible parameter from an experimental point of view) via a bias voltage, we better comprehended the solutions in phase space and the bistability regions. Another important conclusion is the confirmation that multistability could be controlled by means of a secondary sinusoidal perturbation. The key feature of this open-loop strategy was its phase dependence. This new aspect was highlighted in the case of the resonance condition 1:1 between the two frequencies. The phase and amplitude of the perturbation constituted the parameter space for controlling multistability. This control strategy could be implemented in experiments employing a slightly detuning, Δf, of the resonance condition. This detuning implies a continuous phase shift of 2π in a time interval $\Delta T = 1/\Delta f$. The phase control strategy for multistability was

proved for both cases, i.e., when the two solutions were periodic and when one was periodic and the other chaotic. It emerged that controlling chaotic multistability requires less energy (proportional to the square of perturbation amplitude) than periodic multistability. The stabilized solution was the one characterized by less dissipativity. The above general considerations are of fundamental importance for applications involving multistability.

DEDICATION

This paper is dedicated to the memory of Professor Tito Arecchi (1933-2021), the pioneer in the field of laser instabilities.

AUTHOR DECLARATIONS

Conflict of Interest

The authors have no conflicts to disclose.

DATA AVAILABILITY

The data that support the findings of this study are available from the corresponding author upon reasonable request.

REFERENCES

[1]F. T. Arecchi, R. Meucci, G. Puccioni, and J. Tredicce, "Experimental evidence of subharmonic bifurcations, multistability, and turbulence in a Q-switched gas laser," Phys. Rev. Lett. **49**(17), 1217–1220 (1982).
[2]U. Feudel, "Complex dynamics in multistable systems," Int. J. Bifurcation Chaos **18**(6), 1607–1626 (2008).
[3]U. Feudel, A. N. Pisarchik, and K. Showalter, "Multistability and tipping: From mathematics and physics to climate and brain—Minireview and preface to the focus issue," Chaos **28**, 033501 (2018).
[4]J. M. Saucedo-Solorio, A. N. Pisarchik, A. V. Kir'yanov, and V. Aboites, "Generalized multistability in a fiber laser with modulated losses," J. Opt. Soc. Am. B **20**, 490–496 (2003).
[5]A. N. Pisarchik, R. Jaimes-Reategui, R. Sevilla-Escoboza, G. Huerta-Cuellar, and M. Taki, "Rogue waves in a multistable system," Phys. Rev. Lett. **107**, 274101 (2011).
[6]J.-L. Schwartz, N. G. Rimault, J.-M. Hupe, B. Moore, and D. Pressnitzer, "Multistability in perception: Binding sensory modalities, an overview," Philos. Trans. R. Soc. B **367**, 896–905 (2012).
[7]L. Ryashko, "Sensitivity analysis of the noise-induced oscillatory multistability in Higgins model of glycolysis," Chaos **28**, 033602 (2018).
[8]V. Lucarini and T. Bodai, "Edge states in the climate system: Exploring global instabilities and critical transitions," Nonlinearity **30**, R32–R66 (2017).
[9]R. May, "Thresholds and breakpoints in ecosystems with multiplicity of stable states," Nature **269**, 471–477 (1977).
[10]M. Ciofini, A. Politi, and R. Meucci, "Effective two-dimensional model for CO_2 lasers," Phys. Rev. A **48**, 605–610 (1993).
[11]R. Meucci, S. Euzzor, F. T. Arecchi, and J.-M. Ginoux, "Minimal universal model for chaos in a laser with feedback," Int. J. Bifurcation Chaos **31**(4), 2130013 (2021).
[12]L. Ricci, A. Perinelli, M. Castelluzzo, S. Euzzor, and R. Meucci, "Experimental evidence of chaos generated by a minimal universal oscillator model," Int. J. Bifurcation Chaos **31**(12), 2150205 (2021).
[13]A. N. Pisarchik and U. Feudel, "Control of multistability," Phys. Rep. **540**(4), 167–218 (2014).
[14]A. N. Pisarchik and B. K. Goswami, "Annihilation of one of the coexisting attractors in a bistable system," Phys. Rev. Lett. **84**(7), 1423 (2000).
[15]A. N. Pisarchik, "Controlling the multistability of nonlinear systems with coexisting attractors," Phys. Rev. E **64**(4), 046203 (2001).
[16]A. N. Pisarchik and B. F. Kuntsevich, "Control of multistability in a directly modulated diode laser," IEEE J. Quantum Electron. **38**(12), 1594–1598 (2002).
[17]A. N. Pisarchik, Y. O. Barmenkov, and A. V. Kir'yanov, "Experimental demonstration of attractor annihilation in a multistable fiber laser," Phys. Rev. E **68**(6), 066211 (2003).
[18]B. K. Goswami and A. N. Pisarchik, "Controlling multistability by small periodic perturbation," Int. J. Bifurcation Chaos **18**(6), 1645–1673 (2008).
[19]E. N. Egorov and A. A. Koronovskii, "Dynamical control in multistable systems," Tech. Phys. Lett. **30**(3), 186–189 (2004).
[20]R. Meucci, W. Gadomski, M. Ciofini, and F. T. Arecchi, "Experimental control of chaos by means of weak parametric perturbations," Phys. Rev. E **49**(4), R2528–R2531 (1994).
[21]R. Meucci, S. Euzzor, E. Pugliese, S. Zambrano, M. R. Gallas, and J. A. C. Gallas, "Optimal phase-control strategy for damped-driven Duffing oscillators," Phys. Rev. Lett. **116**(4), 044101 (2016).
[22]F. T. Arecchi, W. Gadomski, and R. Meucci, "Generation of chaotic dynamics by feedback on a laser," Phys. Rev. A **34**(2), 1617–1620 (1986).
[23]F. T. Arecchi, R. Meucci, and W. Gadomski, "Laser dynamics with competing instabilities," Phys. Rev. Lett. **58**(21), 2205-–2208 (1987).
[24]C. Grebogi, E. Ott, and J. A. Yorke, "Crises: Sudden changes in chaotic attractors and chaotic transients," Physica D **7**, 181–200 (1983).
[25]U. Feudel, C. Grebogi, B. R. Hunt, and J. A. Yorke, "Map with more than 100 coexisting low-period periodic attractors," Phys. Rev. E **54**, 71–81 (1996).
[26]R. Meucci, A. Poggi, F. T. Arecchi, and J. R. Tredicce, "Dissipativity of an optical chaotic system characterized via generalized multistability," Opt. Commun. **65**, 151–156 (1988).
[27]J. C. Sprott, *Chaos and Time-Series Analysis* (Oxford University Press, 2003).
[28]E. Ott, *Chaos in Dynamical Systems* (Cambridge University Press, 1993).
[29]J. C. Sprott, "A proposed standard for the publication of new chaotic systems," Int. J. Bifurcation Chaos **21**(09), 2391–2394 (2011).
[30]A. Jafari, I. Hussain, F. Nazarimehr, S. M. R. H. Golpayegani, and S. Jafari, "A simple guide for plotting a proper bifurcation diagram," Int. J. Bifurcation Chaos **31**(1), 2150011 (2021).
[31]A. Wolf, J. B. Swift, H. L. Swinney, and J. A. Vastano, "Determining Lyapunov exponents from a time series," Physica D **16**(3), 285–317 (1985).
[32]J. D'Alembert, "Suite des recherches sur le calcul intégral, quatrième partie: Méthodes pour intégrer quelques équations différentielles," Hist. Acad. Berlin **4**, 275–91 (1748).